Two-dimensional metamaterials as meta-foams for optimized surface-enhanced solar steam generation

Lan Gao, Elyes Nefzaoui, Frédéric Marty, Xueyong Wei, Stéphane Bastide, Yamin Leprince-Wang, Tarik Bourouina

Version of Record: https://www.sciencedirect.com/science/article/pii/S0927024822002136
Manuscript_d7f655e0cd80dd7e53944179e01745aa

Two-dimensional metamaterials as meta-foams for optimized surface-enhanced solar steam generation

Lan GAO[1], Elyes NEFZAOUI[1], Frédéric MARTY[1], Xueyong WEI[2], Stéphane BASTIDE[3], Yamin LEPRINCE-WANG[1], Tarik BOUROUINA[1]**

[1] ESYCOM lab., Univ Gustave Eiffel, CNRS, F-77454 Marne-la-Vallée, France
[2] School of Mechanical Engineering, Xi'An Jiaotong University, Xi'An, 710049, China
[3] ICMPE, UMR 7182 CNRS-Université Paris Est Créteil, F-94320 Thiais, France

*Corresponding authors: elyes.nefzaoui@esiee.fr ; tarik.bourouina@esiee.fr

We report on a new class of metamaterials, which consists of meta-foams, optimized for high performance in enhanced solar steam generation. The design of these meta-foams involves precise dimensional control of a periodic two-dimensional micro-pore array. Proof-of-concept of meta-foams efficiency is demonstrated using two fabrication technologies. The first one involves microscale plasma etching onto a nanostructured black silicon substrate. As an alternative low-cost technique, we also use 3D printing of a graphene-containing polymer material. The experimental validation shows that the best evaporation rate reaches 1.34 kg/(h·m^2) under 1 sun illumination, in open-air conditions under normal temperature and relative humidity conditions of 20°C and 58%, an unmatched value so far under similar conditions, while the theoretical limit is estimated at 1.5 kg/(h·m^2). This corresponding to a 89 % conversion efficiency. Experimental data concur well with the predicted performance obtained by numerical simulations. The proposed model simultaneously accounts for both heat and mass transfer, including photothermal conversion and water phase change, to guide the optimization towards the maximization of the evaporation rate, an important figure of merit in many applications, including solar heat harvesting and solar water purification.

Keywords: 2D-metamatrial, metafoam, enhanced solar steam generation, evaporation rate, optimization, water purification, solar energy.

1. Introduction

Solar distillation is considered to be one of the most effective approaches for water purification[1]–[5]. In addition, the utilization of solar energy makes the water purification process environmentally friendly. On the other hand, the required facilities and equipment for this process are relatively easy to install and operate. For these reasons, solar distillation technology has drawn the attention of many research groups over the past few decades. To achieve high efficiency solar distillation, several solutions have been proposed such as pre-heated methods[6][7], nocturnal heated methods[8][9] or methods coupled with additional heat sources to increase the system operating temperature[10]–[13]. Enhanced Solar Steam Generation (SSG) with a Black Absorber Sheet (BAS) is one of these methods[14]. To improve the efficiency of the SSG, many efforts have been done by different research groups. A first option is to use the most appropriate materials regarding their intrinsic properties. As the evaporation only occurs at the air-water interface, with the help of a BAS, SSG efficiency can be increased by localizing the heating process at this interface and reducing the water reservoir bulk heating which does not directly contribute to the evaporation process and can thus be considered as a loss mechanism that needs to be minimized. A second option is to increase the steam generation efficiency by improving the ambient conditions during the evaporation, such as reducing locally the ambient humidity, increasing the incident solar radiation power density by concentration[15] and providing airflow by forced convection [16]. For example, in Guo's work[16], a chamber with induced airflow during the evaporation was used to further boost the steam generation efficiency. The ambient operation conditions strongly depend on the experimental setup used by different researchers, the geographical location, seasons, weather and other factors that can boost the intrinsic performance. Therefore, in this work, we will exclusively evaluate the evaporation performance of the BAS itself in SSG in an open-air environment subject only to natural convection, under 1 sun illumination, a temperature of 25°C and an average relative humidity around 50%.

When it comes to the evaporation performance of the BAS, it has been experimentally proven recently that a micro-scale porous-structured BAS improves the SSG efficiency by switching from bulk heating to surface heating[14][17][18]. The BAS plays two key roles: on one hand, a maximized heating because of the BAS high absorptivity, on the other hand, a localized heating due to a superior thermal insulation which reduces the conductive heat loss in the water bulk through the BAS porous structure. In the simple case of a single layer BAS, these two functionalities are ensured by the same material. Recently, a more sophisticated strategy separating the two functions with a bilayer BAS in SSG was proposed and proved to improve the efficiency of steam generation[19]. The top layer material is a high absorptivity photothermal layer where light-to-heat conversion is localized. The second layer material is a low thermal conductivity porous medium, which ensures water imbibition and reduces heat loss into the water column.

Different BAS materials have been studied for SSG, such as polyurethane[20]–[22], graphene oxide[23]–[27], graphene[28][29], and some other porous bio-materials[30]–[34]. Utilizing the advantages of commercial and natural porous materials, BAS can be manufactured simply and quickly through carbonization or other chemical methods to achieve high-efficiency SSG. However, in all previous reports, the porous materials were taken as they are with their actual porosity and physical properties, most of the time with a random distribution of the pores size and their location, which might be good enough but not optimum. To overcome this limitation, some researchers explored different fabrication methods such as 3D printing to fabricate steam generators with different porous structures[18][35]. In addition to the porous structure, an optimized BAS-assisted SSG requires high photothermal performance as well. This is precisely the aim of this work targeting the design, fabrication and experimental evaluation of an optimized meta-foam, which consists of a new class of metamaterials with two-dimensional

periodicity as illustrated in **Figure 1**a, with appropriate control of pores dimension and their surface density.

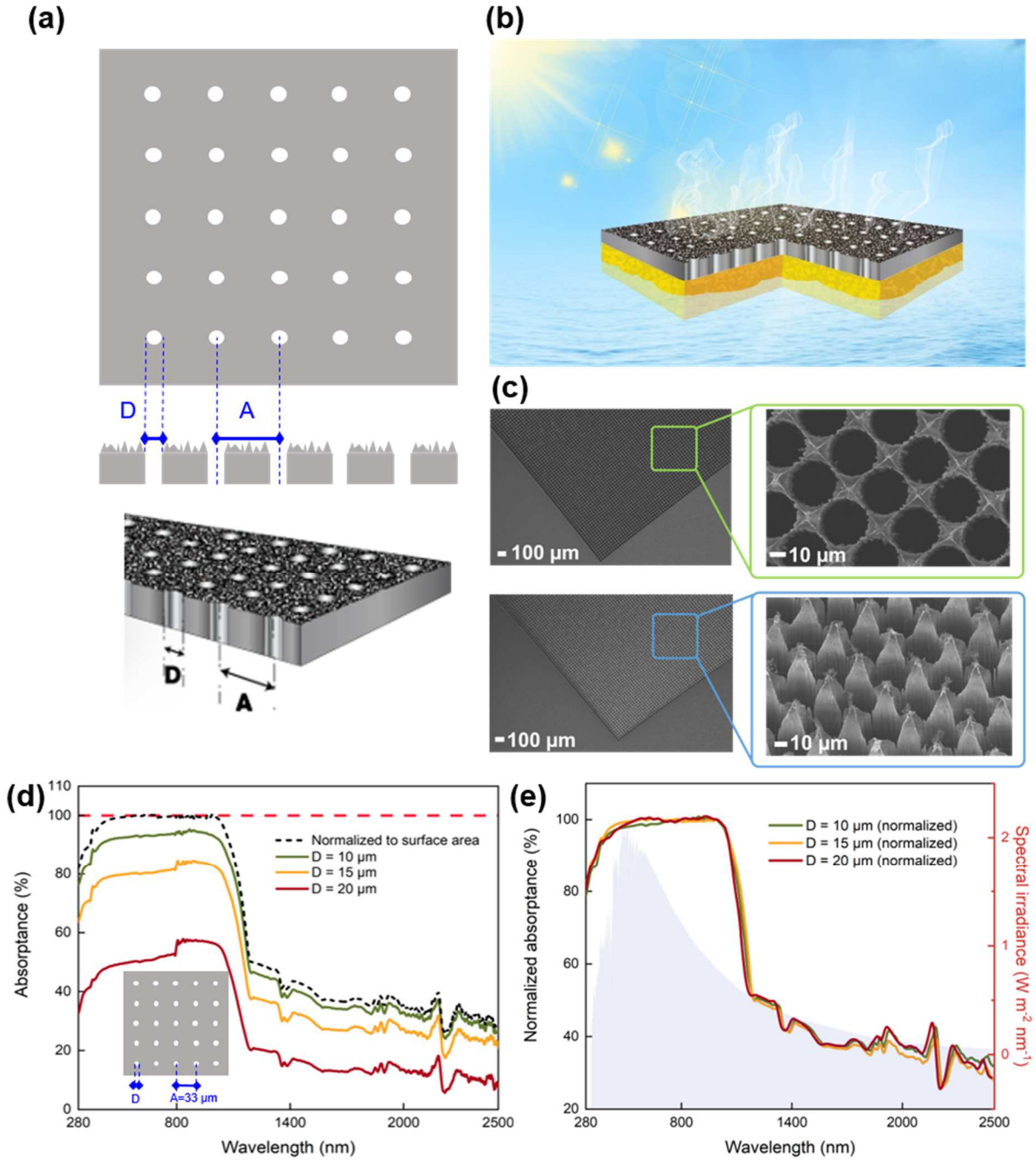

Figure 1. Conceptual schematic representation of the meta-foam: (a) an optimized metamaterial made of a 2D periodic structure, (b) its use for enhanced solar steam generation. (c) SEM images of the fabricated meta-foam made of periodic micro-holes on nanostructured black

silicon. Measured absorptance spectra: (d) raw measurements on different porous surfaces, (e) effective absorptance of the surfaces exposed to solar radiation.

The metafoam is made from an appropriate core material, which should exhibit specific properties, including, a high absorptivity for efficient photothermal conversion of the incident solar radiation reaching the surface. As a first candidate, we selected nanostructured black silicon (B-Si), which has an excellent absorptivity in the solar spectrum from UV-Vis to NIR[36][37],. Then, further microscale drilling of such material can produce the optimum porosity. **Figure 1c** illustrates the resulting hierarchical nano-structuration and micro-structuration with two-dimensional periodicity, obtained from plasma processing of silicon to accommodate for both requirements of excellent absorptivity and optimum porosity for the meta-foam. The function of the high aspect ratio nano-structures is to ensure a very high absorptivity of the resulting black silicon over most of the solar spectrum. **Figure 1**e shows the effective absorptance obtained after measurement on three different samples with different pore diameters (D = 10 µm, D = 15 µm and D = 20 µm). It reaches almost 100% in the spectral range from 300 nm to 1000 nm, corresponding to maximal solar irradiance. It is worth mentioning that the porosity reduces the surface exposed to solar light. Therefore, the effective absorptance is obtained after a normalization process of the raw measured absorptance spectra shown in **Figure 1**d for the three samples under consideration (See the related calculation in supporting information). The function of the micro-scale cylindrical holes array is to ensure optimal heat and mass transfer to the BAS surface for enhanced SSG. At a first glance, there are two conflicting mechanisms: on the one hand, the holes diameters and their density have to be large enough to ensure enough water mass transfer, by imbibition of the hydrophilic holes and further evaporation upon exposure to local heating of the silicon surface exposed to sun. But on the other hand, those holes should not occupy too much of the surface area that should remain available for the solar light to be absorbed by black silicon for the purpose of producing the

heat required for the evaporation to occur at the vicinity of the surface. Finally, a third function is also required: the thermal conductivity should be small enough to avoid heat dissipation from the surface to the water volume. That is why, we implemented a bilayer system involving a regular foam placed underneath our metafoam, shown in yellow in **Figure 1**b, and whose thickness is large enough to ensure the required thermal insulation. It also provides floatability to the whole system leading to as stable and reliable water imbibition for SSG.

2. Results and Discussion

In this section, we present first, the main results obtained using analytical and numerical models. Using a simple analytical model, we calculate the ultimate evaporation rate that can be obtained in enhanced SSG under direct solar radiation and ideal conditions. Then, we use a numerical model to perform a systematic parametric study of the effect of key parameters on enhanced SSG performances including the top layer absorptivity, the BAS second layer porosity as well as the second layer material thermal conductivity. Optimal properties are obtained and discussed with respect to the properties of common materials that can be used for this application. Second, we present our experimental results. We start by introducing a silicon-based meta-foam, produced according to a metamaterial optimization and its experimental use in a bilayer BAS together with a low-cost commercial porous material. The obtained experimental results are then shown to exhibit very good agreement with our analytical and numerical predictions, while providing beyond state-of-the-art performances. Finally we present additional experimental results obtained on 3D-printed meta-foams, aiming a demonstration of the effectiveness of an alternative low-cost technology for producing high-performance meta-foams for enhanced solar steam-generation.

2.1 Asymptotic theoretical limit of the evaporation rate as a target

If we assume an ideal BAS-assisted enhanced SSG system operating in steady state, where all thermal losses (convective, conductive, and radiative) are neglected and where all incident solar

radiation is absorbed and exclusively used for water evaporation, the water steam flow rate can be given by:

$$\dot{m}_v = \frac{q_{solar}}{L_v} \quad (1)$$

where, $\dot{m}_v$ is the generated vapor mass flow rate per unit surface area, L_v = 2415.9 kJ/kg is the evaporation latent heat (we consider a constant ambient temperature $T_a = 293.15\ K$ and an evaporation temperature of $T_e = 309.15\ K$) and q_{solar} = 1000 W/m^2 (a standard 1 sun illumination for solar applications). Using these different assumptions, we obtain an upper limit for the evaporation rate of 1.5 kg/(h·m^2). This value is the maximal evaporation rate that can be obtained with an ideal enhanced SSG system when solar radiation harvesting is maximized and all losses minimized. We note that this value is one or two orders of magnitude lower than values of the capillary flow rate that can be obtained using common porous media[38] which means that the capillary flow-rate is not a limiting factor. This result also confirms that the evaporation rate is mainly limited by the energy input of the system and thermal losses, which are the bottleneck to be optimized.

2.2 Numerical Modeling and Optimization

The model of BAS-enhanced SSG system is schematically depicted in **Figure 2**a, along with the different parts and related physical phenomena that are taken into account in our numerical simulations (see more details in Materials and Methods). The BAS top layer surface absorptivity is the first key parameter for the system operation since it governs the light-to-heat conversion process of the BAS and therefore determines the total energy input to the system. We plot in **Figure 2**b, the BAS equilibrium temperature and the evaporation flow rate as a function of the surface absorptivity as computed using the multi-physical numerical model which is described in the materials and methods section. Plotted results indicate that the higher the absorptivity the higher the evaporation rate. The evaporation rate increases almost linearly

from 1.25 kg/(h·m^2) to 1.31 kg/(h·m^2) as the absorptivity increases from 0.5 to 0.9. Temperature fields in the system are also shown in **Figure 2**c, d. The maximum temperature is obtained at the top surface of the BAS as expected since this spot is designed as the evaporation site. The BAS top surface temperature also increases gradually form 301 K to 303 K as the surface absorptivity increase from 0.5 to 0.9 while the temperature of the BAS and the entire system are set at 293.15 K as initial simulation conditions. The simultaneous increase of the equilibrium temperature and the evaporation rate can be explained by the dependence of the evaporation latent heat to temperature. This quantity actually decreases with temperature going from 2453.6 kJ/kg at 293 K up to 2256.4 kJ/kg at 373 K. Consequently, an increase of the BAS surface temperature leads to an increase of the evaporation rate. Porosity is another key parameter for bilayer BAS in SSG. In the numerical model, the porosity of the top layer and the second layer are expressed by ε_1 and ε_2, respectively. The B-Si material is used for the top layer metamaterial because of its superior performance in photothermal conversion and the tunability of its porosity ε_1. For the second layer, we used a low-cost commercial material with a porosity ε_2 around 0.88. It can be easily acquired from the market and provides both excellent water absorption and thermal insulation (See properties in Supplementary material). The bilayer effective porosity ε can be regarded as a volume-weighted average of the top porosity ε_1 and the second layer porosity ε_2. A parametric study is conducted in which the average porosity ε is varied from 0.7 to 0.9. As shown in **Figure 2**e, the evaporation rate in the system increases as the porosity increases from 0.7 to 0.86 then decreases for porosity values larger than 0.86. By comparing temperature fields for a bilayer average porosity of 0.76 and 0.86 shown in **Figure 2**f-g, one can note that the evaporation rate is larger at a porosity of 0.86 in spite of a lower surface temperature. The evaporation rate starts increasing linearly as the bilayer effective porosity increase from 0.7 to 0.86. Within this range, the increasing bilayer porosity of the BAS improves the evaporation area since it increases the water-air interface area. On the other hand,

increasing the bilayer porosity decreases the second BAS layer thermal conductivity, which increases the BAS surface equilibrium temperature.

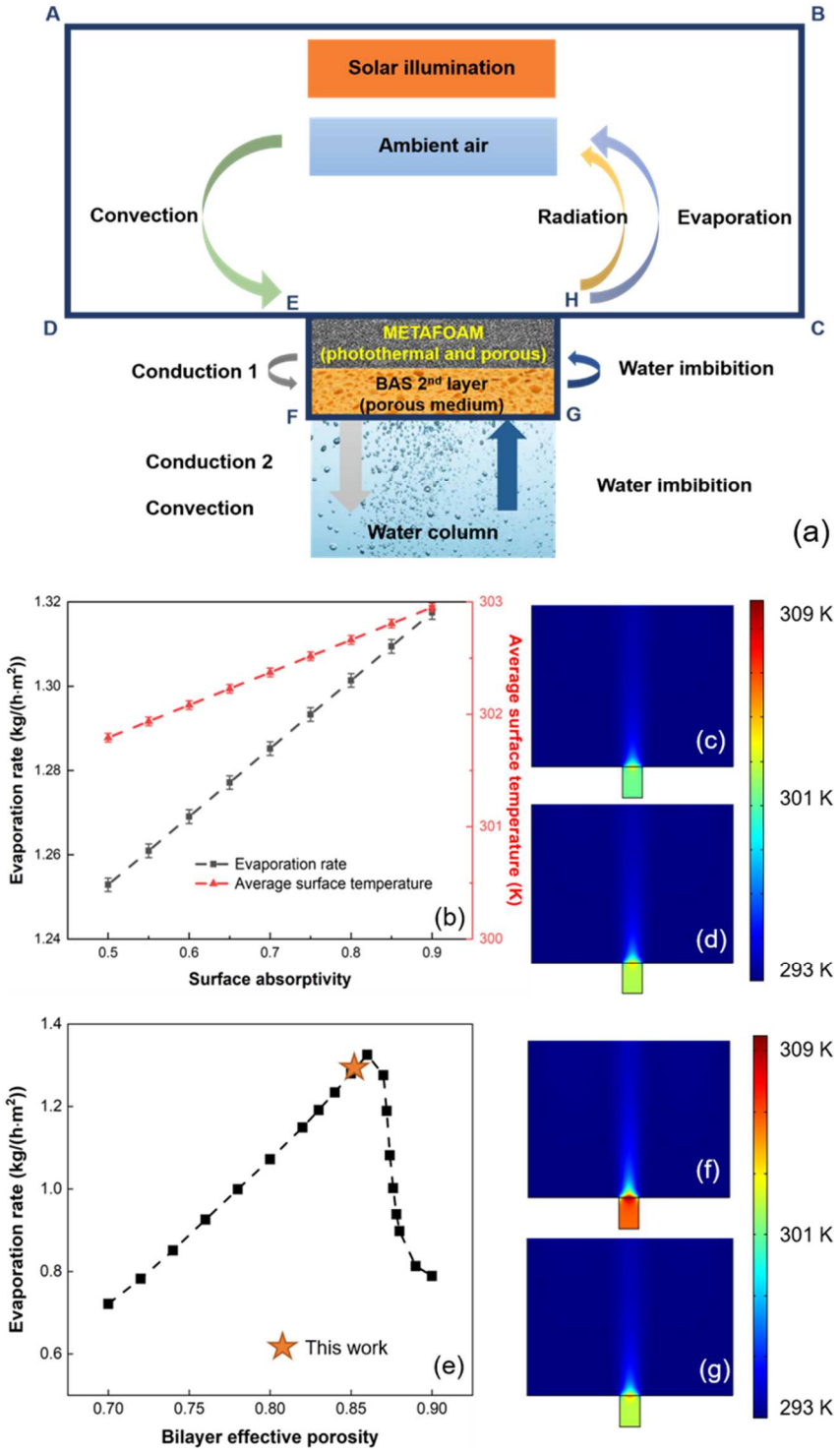

Figure 2. (a) Schematic of a bi-layer BAS-enhanced steam generation device in our numerical model and involved physical phenomena. (b) Simulation results of the BAS surface temperature

at thermal equilibrium as a function of the BAS top layer absorptivity and the temperature field in the system at equilibrium for an absorptivity of (c) 0.5 and (d) 0.9. (e) The evaporation rate as a function of the bilayer effective porosity. (f-g) The temperature fields with a bilayer effective porosity of (g) 0.76 and (h) 0.86 with a surface absorptivity of 0.9.

According to the results shown in **Figure 2**e, an optimized evaporation rate is obtained for a bilayer effective porosity around 0.86 with a top layer surface absorptivity of 0.9. Before the porosity reaches the optimum value, an increasing bilayer effective porosity contributes to a higher evaporation rate. In this region, the increase of the surface area of the water-air interface, which is the evaporation site surface area, dominates which leads to the increasing trend.

The existence of an optimum and the decrease of the evaporation rate when the bilayer effective porosity increases after the maximum can be explained by a competition between two phenomena: (i) the increase of porosity increases the evaporation site surface area and, in the same time; (ii) the decreases of the solar radiation absorption area which is located at the surface of the BAS except at the pores location. Consequently, a porosity increase leads to a reduction of the photothermal conversion sites surface area and reduces the input energy to the system, hence the evaporation rate. From the simulation results, the optimum bilayer effective porosity ε is 0.86. Knowing the thickness of the B-Si layer and the commercial foam (0.4 mm and 15 mm, respectively) and their respective porosities, we calculate the effective porosity of the meta-foam (more information is provided in Materials and Methods section) used in this work and obtain a value of 0.85 as shown on **Figure 2**e.

2.3 Experimental evaluation of the silicon-based 2D meta-foam for enhanced steam generation

The first kind of meta-foams, made solely from silicon, are schematically depicted in **Figure 3**a, and referred to as meta-foams 1. **Figure 3**b shows a photo of the assembly of the square (black) meta-foam 1 on a circular (white) holder with the underlying regular foam (yellow). **Figure 3**c shows the measured evaporation flow rates (see setup in Materials and Methods). The results show that the B-Si meta-foam significantly improves the efficiency of evaporation

compared to water bulk evaporation (violet curve) and compared to a regular commercial foam evaporation (blue curve), both taken as references. Under one sun illumination, the evaporation rate of water bulk and the commercial foam are 0.35 kg/(h·m^2) and 0.76 kg/(h·m^2), respectively. As the diameter of the pores increases in metafoams 1, the porosity of the B-Si layer increases as well as the evaporation rate. For the meta-foam 1 with a diameter D = 10-µm (green curve), D = 15-µm (yellow curve) and D= 20-µm (red curve) perforation, and whose surface area is 1 cm^2, the evaporation rate is 0.94 kg/(h·m^2), 1.08 kg/(h·m^2) and 1.34 kg/(h·m^2) respectively. Periodically perforated B-Si samples with D = 20 µm show the best evaporation rate of 1.34 kg/(h·m^2) which is 3.96 times bigger than that of water bulk evaporation rate. From this result, compared to water bulk evaporation taken as the reference, the efficiency of the SSG has improved from 22.4% to 89.3% under one sun illumination, when adding one of our meta-foams. It is worth mentioning that the evaluation of the efficiency is based on the ultimate upper theoretical limit of 1.50 kg/(h·m^2) as introduced in section 2.1, taken as a reference for 100% efficiency.

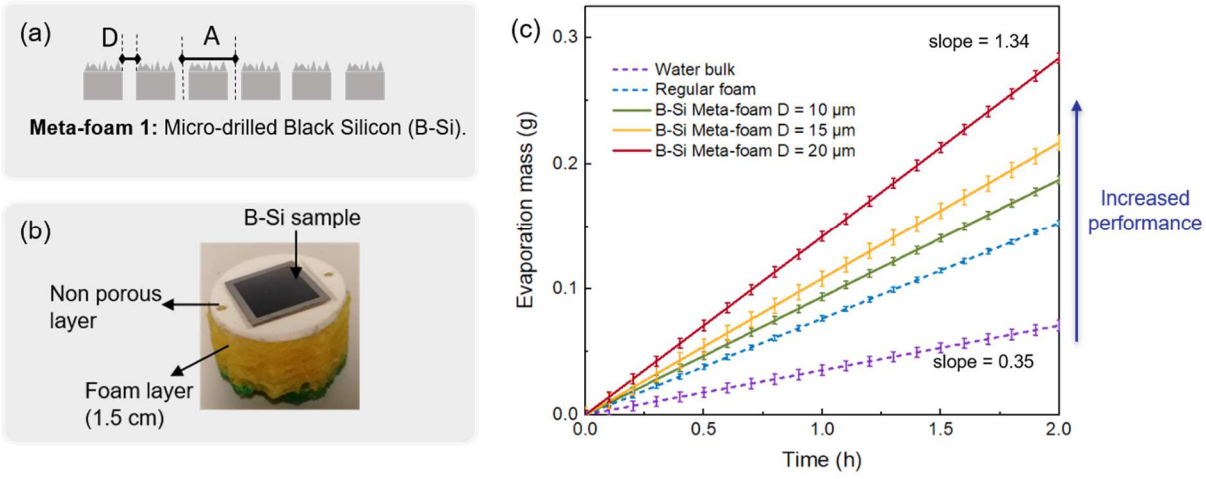

Figure 3. 2D black silicon meta-foams: (a) schematic cross-sectional description, (b) photo of the assembly used for the experiments (c) measured evaporation rates (water loss) on the three different meta-foams, compared with the evaporation rate of bulk water and evaporation rate using a regular foam.

2.4 Experimental evaluation of 3D printed metafoams as a low-cost alternative for enhanced solar-steam generation

Based on the excellent performance of the optimized 2D periodic silicon-based meta-foams, we explored an alternative low-cost technology to produce similar metafoams. The use of 3D printing technology is indeed a promising route towards scalability of such engineered metafoams, although silicon technology is in principle competitive as well in terms of fabrication cost and scalability. Although 3D printing technology has been already used to produce foams based on carbon nanotube graphene oxide (CNT/GO) layers and graphene oxide/nano fibrillated cellulose (GO/NFC) layers [39], our work is a first demonstration of a metafoam involving an array of periodic holes, aiming a precise control of the foam behavior regarding water evaporation. To this end, we launched the fabrication of a set of 3 samples where the hole diameter was the only variable parameter, and whose values were set to D = 100 µm, D = 200 µm and D = 275 µm, all with a fixed spacing of 625 µm and a thickness of 2000 µm. This second kind of meta-foams, are schematically depicted in **Figure 4**a in the form of microporous composite material and is referred to as meta-foams 2.

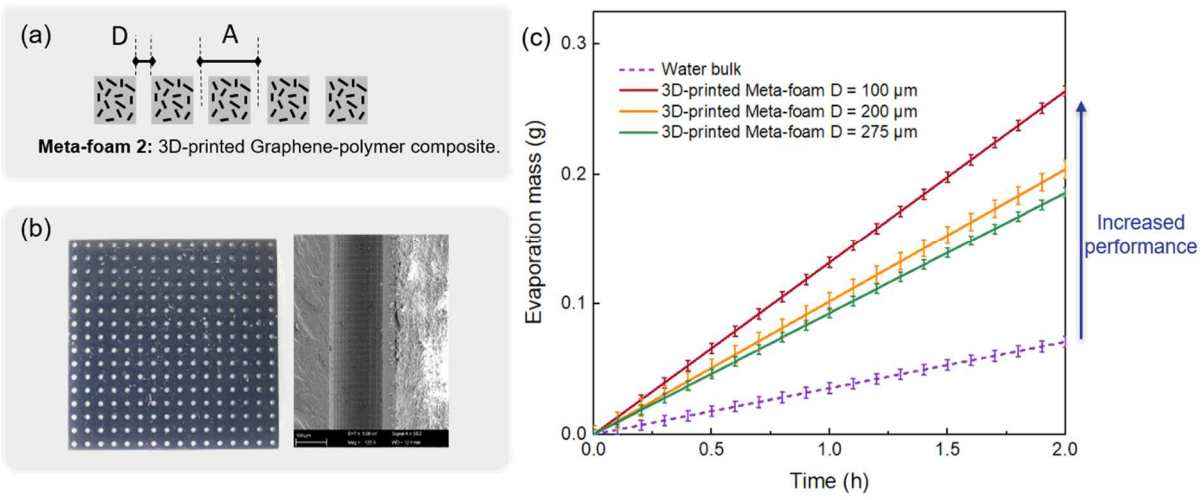

Figure 4. A 3D-printed meta-foam (a) cross-sectional SEM view of one cylindrical micro-pore. The close view reveals the details of the voxel discretization; (b) Measured evaporation rates (water loss) on the three different metafoams, compared with the evaporation rate of bulk water.

Figure 4b shows a cross-sectional SEM view of a single cylindrical micro-pore of the fabricated 3D-printed metafoam. The close view reveals the geometrical feature details, which are typical of the voxel discretization using 3D-printing as an indicator of the spatial resolution. **Figure 4**c shows the measured evaporation flow rates fabricated 3D-printed meta-foams recorded in open-air under one sun illumination. The evaporation rates recorded on meta-foams 2 with a pore diameter of 100 µm, 200 µm, 275 µm, are 1.32 kg/(h·m^2), 1.03 kg/(h·m^2), 0.93 kg/(h·m^2), respectively. They also exhibit a significant improvement compared to water bulk evaporation rate. The maximum value of 1.32 kg/(h·m^2) obtained with D = 275 µm is comparable to the best value obtained of B-Si meta-foams.

2.5 Experimental evaluation of 2D metafoams for Seawater Solar Steam Generation

Solar steam generation using seawater was also conducted to support future practical applications of our novel metafoams. In this experiment, we use seawater instead of DI water. To evaluated the samples stability, the metafoams were drenched in seawater for 14-day before a second steam generation performance assessment. The solar steam generation performances before and after the 14-days immersion in seawater are shown in **Figure 5**a. A DI water evaporation experiment was conducted under the same ambient conditions as a reference for comparison. Before the immersion in seawater, the solar steam generation rate of DI water and seawater are 1.31 kg/(h·m^2) and 1.27 kg/(h·m^2), respectively. After the 14-day immersion in seawater, the evaporation rate is 1.18 kg/(h·m^2) for DI water and 1.19 kg/(h·m^2) for seawater. There is around 7%-9% reduction of the meta-foam solar steam generation performance after a 14-day immersion in seawater. This reduction is probably caused by the crystallized salt which fills the perforated pores and reduces both the water pumping channels as well as the evaporation sites. We show in **Figure 5**b and **Figure 5**c microscopy images of our samples before and after the 14-day treatment, respectively, where we obviously observe perforated pores filled with salt crystals in **Figure 5**c, i.e. after 14 days.

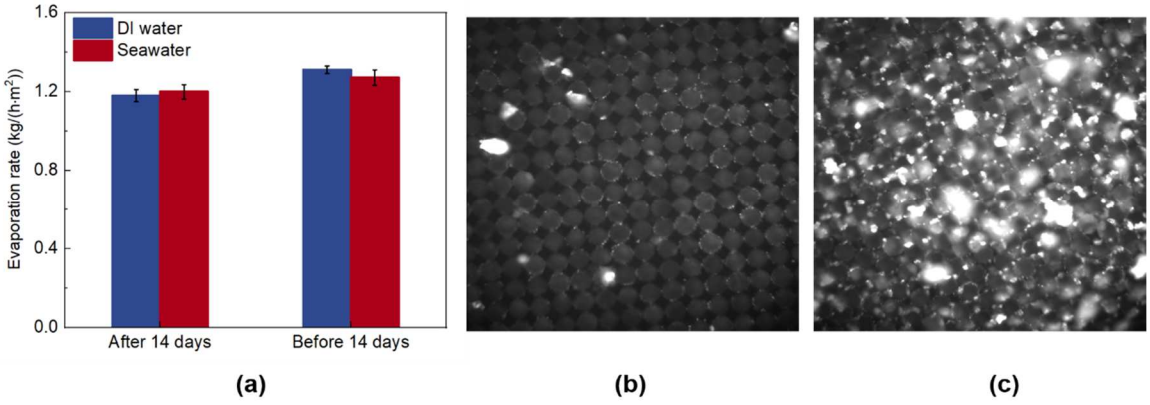

Figure 5. (a) A comparison of seawater evaporation rates and DI water evaporation rates using 2D metafoams and microscopy images of the 2D metafoam surface before (b) and after (c) a 14-day immersion in seawater.

2.6 Evaporation performance comparison

As indicated in the introduction, the evaporation performance of the BAS is highly dependent on the researcher's experimental setup and ambient conditions during the experiments, such as humidity and temperature.

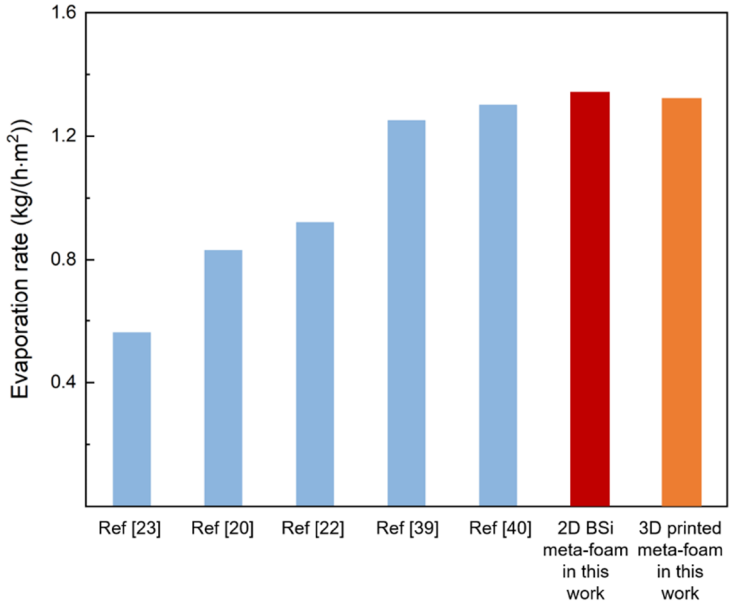

Figure 6. Evaporation rate of the optimal B-Si metafoam and the best 3D-printed graphene-polymer metafoam designed and fabricated in this work, compared to other results from the literature measured under similar experimental conditions, that is under 1 sun illumination and open-air ambient conditions.

Therefore, in **Table 1** and in **Figure 6**, we list and compare our results with previously reported enhanced evaporation results obtained by other groups under similar experimental conditions[20][22][23][39][40] showing that the best performance of this work exceeds the state-of-the-art value among these comparable results.

Table 1. Comparison of evaporation rate values from the literature for SSG obtained under similar conditions, that is under 1 sun illumination and open-air ambient conditions.

Reference title	BAS material	Evaporation rate [kg/(h·m^2)]	Ambient temperature [°C]	Ambient relative humidity [%]
Functionalized Graphene Enables Highly Efficient Solar Thermal Steam Generation[23]	functionalized chemically reduced graphene oxide	0.56	22	60
Recycled waste black polyurethane sponges for solar vapor generation and distillation[20]	hydrophilic treated polyurethane sponges	0.83	20	60
Hydrophobic light-to-heat conversion membranes with self-healing ability for interfacial solar heating[22]	polypyrrole (PPy) coated stainless steel (SS) mesh	0.92	22	50
3D-printed, all-in-one evaporator for high-efficiency solar steam generation under 1 sun illumination[39]	graphene oxide/nanofibrillated cellulose	1.25	20	30
Graphene-based standalone solar energy converter for water desalination and purification[40]	3D cross-linked polymer-like graphene material	1.3	20	25
This work	periodically perforated B-Si 2D meta-foam	1.34	20	58
This work	3D printed meta-foam	1.32	22	36

3. Conclusion

In conclusion, we designed, based on an analytical model and a numerical optimization, an optimized bilayer meta-foam involving the combination of a metamaterial made of periodically perforated black silicon, or, alternatively, made of graphene-containing 3D printed polymer materials, together with a low-cost commercial foam. The key parameters in bilayer black absorbing sheet-assisted solar steam generation have been studied to assess the effect of the most relevant parameters on vapor generation rate for optimization purposes. Obtained results

were applied to the design of an optimized top layer porous structure. Using this class of optimal bilayer meta-foams, we achieved an evaporation rate of 1.34 kg/(h·m^2) using periodically perforated B-Si 2D meta-foam under 1 sun illumination, a value above state-of-the-art. In addition, a 3D printed meta-foam has been fabricated and tested as a low-cost alternative to the B-Si 2D meta-foam, showing a very good performance in SSG as well and high potential for scalability at low-cost. Through this work, it is confirmed that optimized bilayer meta-foams are very promising BAS candidates for enhanced solar steam generation.

4. Materials and Methods

4.1 Steam Generation Experiment

The experimental setup is shown in **Figure 7**a, b. The irradiation source (Oriel® LCS-100TM, Small Area Sol1A, 94011A-ES, AM 1.5 G) provides an incident irradiation of 1kW/m^2 and was calibrated with a solar meter (VOLTCRAFT, PL-110SM) each time before use. The temperature profile was measured using an infrared camera (FLIR, a325sc) and a set of thermocouples (RS 409 - 4908 (PTFE) Thermocouple sensor, Type 'K') connected to a data logger (PICO, TC-08) for data recording. To avoid steam leakage from the water column edge, we cover the reservoir with Teflon tape. The real-time mass loss over the entire experiment duration was recorded using a computer-controlled electronic mass balance (KERN, KB2400-2N) with an accuracy of 0.01g. All SSG experiments were conducted under an ambient temperature at 20±2°C. The relative humidity was 58±2% and 36 ±2%, for black-silicon and 3D-printed metafoams for DI water evaporation, respectively. Both temperature and relative humidity were monitored using a multi-physical sensor (KIMO, AMI 310).

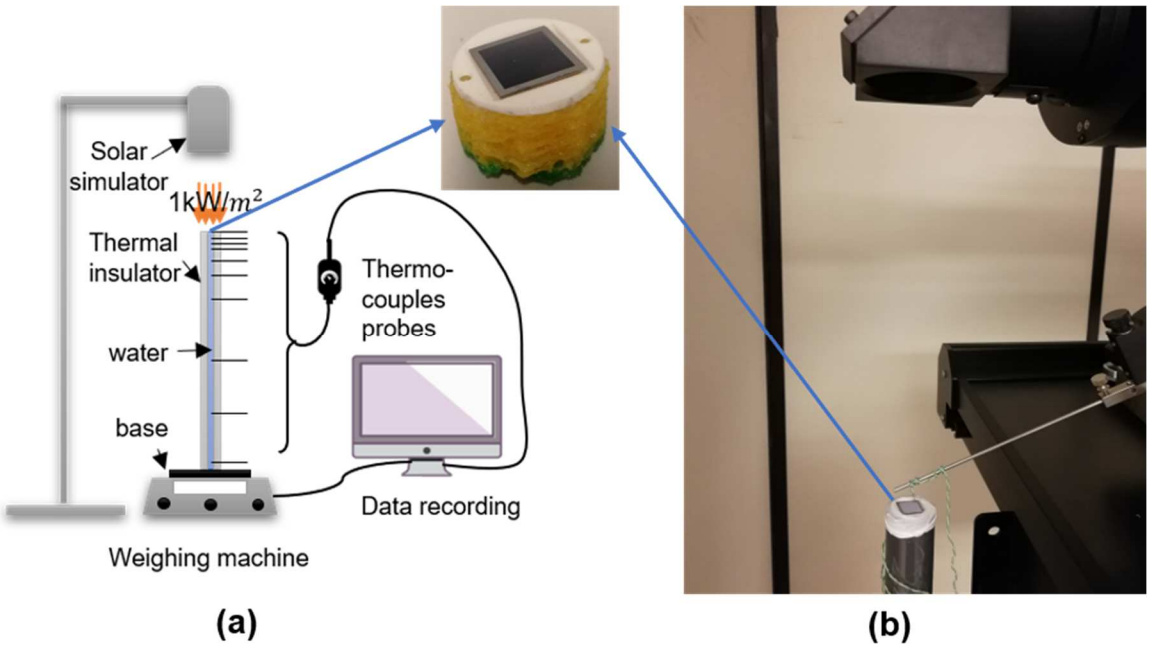

Figure 7. (a) Schematic of the SSG experimental setup. (b-c) Photo of the B-Si meta-foam mounted in the actual experimental setup.

4.2 Seawater Steam Generation Experiment

Seawater samples were prepared using sea salt (ARKA Biotechnologie GmbH) and DI water. The durability and stability of the 2D meta-foams were also tested. For this purpose, the samples were drenched in seawater for 14 days and their solar steam generation performances were compared before and after this manipulation. For seawater evporation, the ambient temperature and the relative humidity was 20±2°C and 45±2%, respectively.

4.3 Fabrication and Characterization of the Meta-foam

4.3.1 High performance B-Si samples

The periodical perforated B-Si was made on a 4-inch diameter, 390±10 µm thick double side polished single-crystalline silicon substrate with (100) orientation with low phosphorous doping (1-5 Ohm-cm electrical resistivity). The meta-foam was produced in a two-step sequence described in **Figure 8,** involving plasma processing of the silicon surface. An aluminum thin film was first deposited by sputtering on both sides of the substrate to serve as a hard mask for the Deep Reactive Ion etching (DRIE) process. A thin layer of photoresist was spun-coated over the aluminum layer and patterned to define the periodic structure on both

sides of the substrate. The pattern was then transferred to the hard mask by Chlorine plasma etch of the aluminum layer. The next step consists of deep silicon etch using a Bosch process in an ALCATEL A601E deep reactive ion etching reactor. The etching process involves a time-multiplexed plasma etch including etch and passivation steps which use SF_6 gas for 5 seconds and sub-steps of sidewall passivation under C_4F_8 gas for 2 seconds. More details can be found for instance in our previous work[41]. The process was stopped when patterns are fully etched through the wafer thickness. Aluminum hard mask was then wet etched to reveal the silicon surface. The final etching step consists of B-Si formation at the top of the periodic patterns and was carried-out in the same plasma reactor configured for cryogenic etching. The process used a SF_6/O_2 chemistry at a temperature of -110 °C where SF_6 was the etching gas and O_2 was used as a catalyst for the passivation of the etched walls. By tuning the SF_6/O_2 ratio, we can obtain a B-Si surface as shown on **Figure 1**c where the SEM images of the B-Si were taken by Zeiss NEON 40 High-Resolution Scanning Electron Microscope (HR-SEM). The fixed parameters were the source power of 1000 W, the pressure of 2 Pa and the bias voltage of 10 V with detailed formation mechanisms described in our previous work[42].

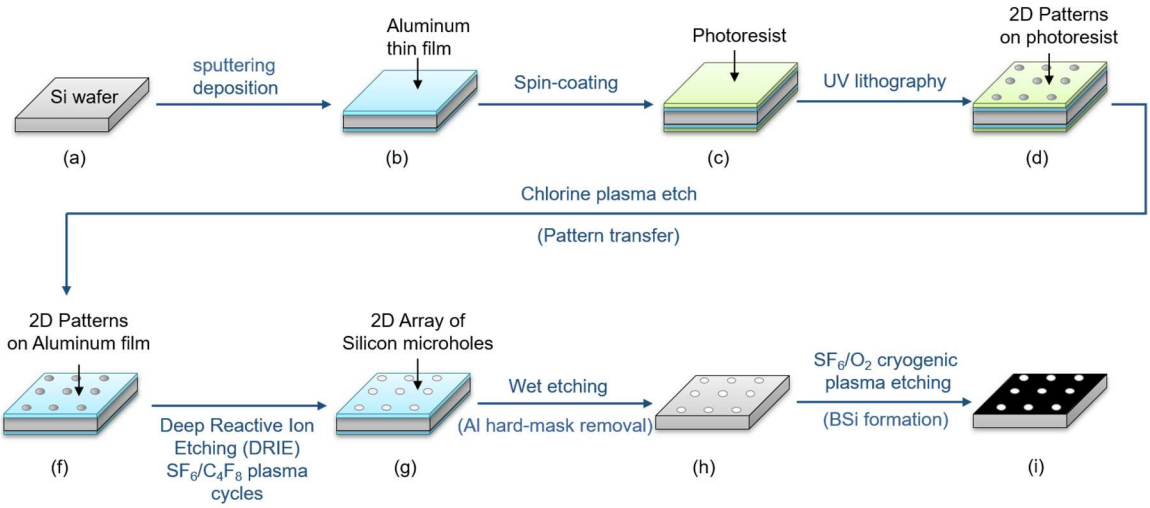

Figure 8. Fabrication sequence to produce the 2D metafoams of type 1 through silicon micro and nanostructuration.

A final dicing step with a DAD350 Disco dicing saw was carried-out to get individual chips. The reflectance and transmittance of the perforated B-Si samples were measured by the UV-Vis-NIR spectrometer (Agilent, Cary 7000). The results shown in **Figure 1**d indicate that the perforated B-Si samples maintain a considerable high absorptance in the UV-Vis range. The raw data can be found in the supplementary material. Those samples were used as the BAS top layer. Samples with three different pore sizes were fabricated: D = 10 μm, D = 15 μm and D = 20 μm, all with the same number of 100 000 pores over an area of 1 cm^2, corresponding to a porosity ε_1 varying from 0.079, 0.177 and 0.314, respectively.

The proposed BSi metafoams have the combined potentials of scalability and low-cost. Indeed, because silicon is the bare material, one benefits from the existing manufacturing infrastructures of the semiconductor industry, which were proven to be cost-effective using scalable fabrication processes for multiple applications including electronic devices and solar cells. At a first glance, based on a comparable number of steps in the fabrication sequence, one can make a rough estimate of the cost considering the use of silicon to produce solar cells. According to the literature [43][44], figures of cost for silicon solar cells are in the order of 1 USD per wafer of 250 cm^2 corresponding to nearly 40 USD per m^2.

4.3.2 Low Cost 3D Printing Samples

Besides the high-performance B-Si samples, we also fabricated the metafoam using the low-cost material by 3D printing technology. With the STereo-Lithography (STL) files, the samples are fabricated using the NANOArch® S130 from BOSTON MICRO FABRICATION, which can realize high-precision large-format micro-scale 3D printing. Taking advantage of PμSL (Projection Micro Stereolithography) technology, the equipment uses a high-precision UV lithography projection system to project the pattern to be printed on the liquid surface of the resin tank, solidify the resin on the liquid surface and directly process three-dimensional and complex shapes from the digital model to complete the samples production. The available

printing materials are diverse. Since the temperature of the sample surface may significantly increase during the evaporation process, we selected a high temperature resistant material (HTL), to fabricate our 3D-printed metafoam. This material consists of a composite produced by a dispersion of graphene in a polymer matrix.

4.3.3 Bilayer metafoam assembly

The commercial porous material was cut into a 2 cm-diameter cylindrical shape with a thickness of 1.5 cm to fit the experimental reservoir. By referring to other enhanced steam generation works in the literature[30][31][45][46], the pore size of common natural porous media materials is generally 5 to 50 µm. In order to obtain a full contact between the commercial porous material and the perforated B-Si samples, a 3D printed cover was designed and fabricated according to the shape of the perforated B-Si samples using white polylactic acid (PLA) material. Good attachment and tightness have been ensured by using several auxiliary layers of Teflon tape.

4.4 Multi-physical Numerical Model

In this numerical model, the capillary transport in the porous foam and the water vapor transport are modeled using empirical equations[47]. The water evaporation at the meta-foam surface is described by a diffusion model using Millington and Quirk equation[48]. Species transport equations are coupled to Navier-Stokes equations for convective heat transfer modeling, where the thermal properties of the porous foam are taken into account[49][50]. The entire process of steam transport in ambient air is spontaneous and not assisted by forced convection for vapor evacuation, which means it is ensured by species concentration diffusion and natural convection which results from the temperature difference between the BAS surface and the ambient air. Compared to previously reported works[51], we use laminar flow temperature-dependent compressible Navier-Stokes equations in our model which is implemented in a multi-physical commercial simulation software, COMSOL Multiphysics for instance.

As shown in **Figure 2**a, we consider a two-dimensional (2D) geometry where we can clearly distinguish a bilayer BAS block (EHGF) and an ambient air block (ABCD). The BAS block is 15 mm thick and 10 mm wide. It is nested in a larger air block which dimensions are 150 x 100 mm^2. To simplify the model, we make the following assumptions: (1) The thickness of the BAS photothermal functional surface is negligible compared to the total thickness of the BAS; (2) Radiative losses are located in the surface of the BAS only; (3) The porous medium of the BAS is isotropic; (4) Ambient air humidity is constant, hence not affected by generated steam. This requires an efficient evacuation of water vapor from the BAS surface; (5) Only natural convection is accounted for at the BAS surface. Boundary conditions used for simulation are listed in supplementary material.

Acknowledgements
This project received the support from the I-SITE FUTURE Initiative (reference ANR-16-IDEX-0003) in the frame of the project NANO-4-WATER as well as the METAWATER Project (ANR-20-CE08-0023 META-WATER).

Received: ((will be filled in by the editorial staff))
Revised: ((will be filled in by the editorial staff))
Published online: ((will be filled in by the editorial staff))

References

[1] B. Chaouchi, A. Zrelli, S. Gabsi, *Desalination* **2007**, *217*, 118.
[2] S. Sharma, A. Bhattacharya, *Applied Water Science* **2017**, *7*, 1043.
[3] C. Tenthani, A. Madhlopa, C.Z.M. Kimambo, **2012**.
[4] G.N. Tiwari, H.N. Singh, R. Tripathi, *Solar Energy* **2003**, *75*, 367.
[5] L. Ye, H. You, J. Yao, H. Su, *Desalination* **2012**, *298*, 1.
[6] L. García-Rodríguez, C. Gómez-Camacho, *Desalination* **1999**, *126*, 109.
[7] Y.P. Yadav, *Desalination* **1993**, *91*, 135.
[8] G.S. Dhindsa, M.K. Mittal, *Energy Conversion and Management* **2018**, *165*, 669.
[9] P. Naveen Kumar, D.G. Harris Samuel, P.K. Nagarajan, R. Sathyamurthy, *International Journal of Ambient Energy* **2017**, *38*, 694.
[10] T. Arunkumar, D. Denkenberger, R. Velraj, R. Sathyamurthy, H. Tanaka, K. Vinothkumar, *Energy Conversion and Management* **2015**, *105*, 665.
[11] M.A. Eltawil, Z.M. Omara, *Desalination* **2014**, *349*, 1.
[12] A.E. Kabeel, M. Abdelgaied, *Solar Energy* **2017**, *144*, 71.
[13] G.M. Zaki, A. Al-Turki, M. Al-Fatani, *Solar Energy* **1992**, *11*, 193.
[14] G. Ni, G. Li, S.V. Boriskina, H. Li, W. Yang, T. Zhang, G. Chen, *Nature Energy* **2016**, *1*, 1.
[15] M. Zhu, Y. Li, F. Chen, X. Zhu, J. Dai, Y. Li, Z. Yang, X. Yan, J. Song, Y. Wang, *Advanced Energy Materials* **2018**, *8*, 1701028.
[16] Y. Guo, X. Zhou, F. Zhao, J. Bae, B. Rosenberger, G. Yu, *ACS Nano* **2019**, *13*, 7913.
[17] W. Li, X. Tian, X. Li, S. Han, C. Li, X.-Z. Zhai, Y. Kang, Z.-Z. Yu, *Journal of Materials Chemistry A* **2021**, *9*, 14859.
[18] M. He, H. Dai, H. Liu, Q. Cai, Y. Liu, L. Wang, X. Qin, J. Yu, *ACS Applied Materials & Interfaces* **2021**, *13*, 40664.
[19] H. Ghasemi, G. Ni, A.M. Marconnet, J. Loomis, S. Yerci, N. Miljkovic, G. Chen, *Nature Communications* **2014**, *5*, 4449.
[20] S. Ma, C.P. Chiu, Y. Zhu, C.Y. Tang, H. Long, W. Qarony, X. Zhao, X. Zhang, W.H. Lo, Y.H. Tsang, *Applied Energy* **2017**, *206*, 63.
[21] F.F. Gong, H. Li, W. Wang, J. Huang, D.D. Xia, J. Liao, M. Wu, D.V. Papavassiliou, *Nano Energy* **2019**, *58*, 322.
[22] L. Zhang, B. Tang, J. Wu, R. Li, P. Wang, *Advanced Materials* **2015**, *27*, 4889.
[23] J. Yang, Y. Pang, W. Huang, S.K. Shaw, J. Schiffbauer, M.A. Pillers, X. Mu, S. Luo, T. Zhang, Y. Huang, *ACS Nano* **2017**, *11*, 5510.
[24] X. Hu, W. Xu, L. Zhou, Y. Tan, Y. Wang, S. Zhu, J. Zhu, *Advanced Materials* **2017**, *29*, 1604031.
[25] G. Wang, Y. Fu, A. Guo, T. Mei, J. Wang, J. Li, X. Wang, *Chemistry of Materials* **2017**, *29*, 5629.
[26] X. Li, W. Xu, M. Tang, L. Zhou, B. Zhu, S. Zhu, J. Zhu, *Proceedings of the National Academy of Sciences* **2016**, *113*, 13953.
[27] W. Li, X. Li, W. Chang, J. Wu, P. Liu, J. Wang, X. Yao, Z.-Z. Yu, *Nano Research* **2020**, *13*, 3048.
[28] P. Zhang, J. Li, L. Lv, Y. Zhao, L. Qu, *Acs Nano* **2017**, *11*, 5087.
[29] Y. Ito, Y. Tanabe, J. Han, T. Fujita, K. Tanigaki, M. Chen, *Advanced Materials* **2015**, *27*, 4302.
[30] N. Xu, X. Hu, W. Xu, X. Li, L. Zhou, S. Zhu, J. Zhu, *Advanced Materials* **2017**, *29*, 1606762.
[31] G. Xue, K. Liu, Q. Chen, P. Yang, J. Li, T. Ding, J. Duan, B. Qi, J. Zhou, *ACS Applied Materials & Interfaces* **2017**, *9*, 15052.

[32] M. Zhu, Y. Li, G. Chen, F. Jiang, Z. Yang, X. Luo, Y. Wang, S.D. Lacey, J. Dai, C. Wang, *Advanced Materials* **2017**, *29*, 1704107.
[33] Y. Geng, W. Sun, P. Ying, Y. Zheng, J. Ding, K. Sun, L. Li, M. Li, *Advanced Functional Materials* **2020**, 2007648.
[34] W. Li, X. Tian, X. Li, J. Liu, C. Li, X. Feng, C. Shu, Z.-Z. Yu, *Journal of Colloid and Interface Science* **2022**, *606*, 748.
[35] S. Zhou, S. Huang, Y. Ming, Y. Long, H. Liang, S. Ruan, Y.-J. Zeng, H. Cui, *Journal of Materials Chemistry A* **2021**, *9*, 9909.
[36] S. Sarkar, A.A. Elsayed, E. Nefzaoui, J. Drevillon, P. Basset, F. Marty, M. Anwar, Y. Yu, J. Zhao, X. Yuan, in *2019 IEEE 32nd International Conference on Micro Electro Mechanical Systems (MEMS)*, IEEE**2019**, 860.
[37] Y. Nishijima, H. Nishijima, S. Juodkazis, *Solar Energy Materials and Solar Cells* **2020**, *217*, 110706.
[38] M. Liu, J. Wu, Y. Gan, D.A. Hanaor, C.Q. Chen, *International Journal of Heat and Mass Transfer* **2018**, *123*, 239.
[39] Y. Li, T. Gao, Z. Yang, C. Chen, W. Luo, J. Song, E. Hitz, C. Jia, Y. Zhou, B. Liu, *Advanced Materials* **2017**, *29*, 1700981.
[40] Y. Yang, R. Zhao, T. Zhang, K. Zhao, P. Xiao, Y. Ma, P.M. Ajayan, G. Shi, Y. Chen, *ACS Nano* **2018**, *12*, 829.
[41] F. Marty, L. Rousseau, B. Saadany, B. Mercier, O. Français, Y. Mita, T. Bourouina, *Microelectronics Journal* **2005**, *36*, 673.
[42] K.N. Nguyen, P. Basset, F. Marty, Y. Leprince-Wang, T. Bourouina, *Journal of Applied Physics* **2013**, *113*, 194903.
[43] M. Fathi, A. Mefoued, A. Messaoud, Y. Boukennous, *Physics Procedia* **2009**, *2*, 751.
[44] A. Louwen, W. Van Sark, R. Schropp, A. Faaij, *Solar Energy Materials and Solar Cells* **2016**, *147*, 295.
[45] M.M. Ghafurian, H. Niazmand, E. Ebrahimnia-Bajestan, R.A. Taylor, *Renewable Energy* **2020**, *146*, 2308.
[46] X. Gao, H. Lan, S. Li, X. Lu, M. Zeng, X. Gao, Q. Wang, G. Zhou, J.-M. Liu, M.J. Naughton, *Global Challenges* **2018**, *2*, 1800035.
[47] J.-G. Choi, D.D. Do, H.D. Do, *Industrial & Engineering Chemistry Research* **2001**, *40*, 4005.
[48] R.J. Millington, J.P. Quirk, *Nature* **1964**, *202*, 143.
[49] A.K. Datta, *Journal of Food Engineering* **2007**, *80*, 80.
[50] A.K. Datta, *Journal of Food Engineering* **2007**, *80*, 96.
[51] J. Zhong, C. Huang, D. Wu, Z. Lin, *International Journal of Heat and Mass Transfer* **2019**, *128*, 860.

A two-dimensional (2D) metamaterial is introduced as a meta-foam based on 2D-arrayed micro-pores drilled on black silicon aiming highly efficient surface-enhanced solar steam generation. Optimization of the design results from multiphysics modelling and simulation. Experimental evaluation under 1 sun illumination shows an evaporation rate up to 1.34 kg/(h·m^2) corresponding to 89% conversion efficiency. Similar meta-foams based on 3D-printed graphene-containing polymers also show similar results based on a low-cost scalable technology.

Dr. L. Gao, Dr. E. Nefzaoui, Eng. F. Marty, Prof. X. Wei, Dr. S. Bastide, Prof. Y. Leprince-Wang, Prof. T. Bourouina

Two-dimensional metamaterials as meta-foams for optimized surface-enhanced solar steam generation